An improved version of the view factor method for simulating inertial confinement fusion hohlraums

Mikhail Basko[a)]
Max-Planck-Institut für Quantenoptik, D-85748 Garching, Germany

(Received 17 April 1996; accepted 5 August 1996)

A modified version of the view factor equations is proposed which improves the accuracy of the description of temporal effects in energy redistribution by thermal radiation in cavities driven by power pulses typical for inertial confinement fusion (ICF). The method is applied to analyze the process of radiative symmetrization in the simplest type of closed cylindrical hohlraums heated by two x-ray rings on the sidewall of the hohlraum case. Such hohlraums may be used in certain types of ICF targets driven by ion beams. © *1996 American Institute of Physics.*
[S1070-664X(96)02411-1]

I. INTRODUCTION

Indirect drive approach to inertial confinement fusion (ICF) is based on the concept of radiation cavity—a hohlraum.[1] The driving laser or particle beams generate thermal x rays inside a high-Z cavity case. These x rays are repeatedly absorbed and reemitted by the case walls and deposit their energy upon the surface of a spherical fusion capsule inside the hohlraum in a nearly perfectly symmetric way. However, for any particular type of an ICF target, the hohlraum configuration must be carefully designed to provide the necessary symmetry of capsule irradiation.[2] An effective practical method for calculating radiative energy redistribution in hohlraums, particularly suitable for the initial stage of hohlraum optimization, is based on a ''view factor'' approach.[3–6]

A major drawback of the original system of the view factor equations, as proposed in Refs. 3–6, is associated with poor accuracy in describing temporal effects for non-power-law variations of the source power. In Sec. II it is shown how these equations can be modified to render a much more accurate description of hohlraums with sudden increases of the driving power. Section III describes briefly how the values of the reemission parameters, which enter the view factor equations, can be calculated for different materials.

In Sec. IV, the modified system of the view factor equations is applied to analyze the temporal behavior of the low-order asymmetry modes in closed cylindrical hohlraums heated by two ring sources of x rays. Such hohlraums may provide an interesting option for ICF targets driven by the beams of heavy ions.[7,8] The time-dependent effects due only to multiple reemission by the hohlraum walls and capsule surface are analyzed. The neglect of the plasma blowoff effects is partly justified by relatively large hohlraum dimensions considered. To make an easy comparison with the laser target proposed for the National Ignition Facility (NIF),[2] a fusion capsule of the same size $R_c=1.11$ mm, and the x ray pulse of approximately the same shape and the same energy as in the NIF target are used in all the numerical simulations.

[a)]On leave from the Institute for Theoretical and Experimental Physics, B. Cheremushkinskaya 25, 117259 Moscow, Russia. Electronic mail: basko@vitep3.itep.ru

II. VIEW FACTOR EQUATIONS

The view factor equations express the energy balance for each surface element inside a radiation cavity in the form

$$S_a(t,\mathbf{r})+S_r(t,\mathbf{r})=S_q(t,\mathbf{r})+\int_A V_f(\mathbf{r},\mathbf{r}')S_r(t,\mathbf{r}')dA', \tag{1}$$

where $S_a(t,\mathbf{r})$ and $S_r(t,\mathbf{r})$ are, respectively, the fluxes of the absorbed and reemitted radiation (per unit surface area), $S_q(t,\mathbf{r})$ is the radiation flux received from the external sources, and dA' is the surface element at point $\mathbf{r}'$ (for more details see Ref. 6). Under the assumption of Lambertian (isotropic) reemission, the view vactor $V_f(\mathbf{r},\mathbf{r}')$ is given by

$$V_f(\mathbf{r},\mathbf{r}')=-\frac{(\mathbf{l}\cdot\mathbf{n})(\mathbf{l}\cdot\mathbf{n}')}{\pi|\mathbf{l}|^4}, \tag{2}$$

where $\mathbf{l}=\mathbf{r}'-\mathbf{r}$, and $\mathbf{n}$ and $\mathbf{n}'$ are the unit normal vectors to the surface elements at $\mathbf{r}$ and $\mathbf{r}'$, respectively. To solve the integral equation (1), it was originally proposed[5,6] to use a power law relationship

$$S_r(t,\mathbf{r})=K_r t^{\alpha'}[S_a(t,\mathbf{r})]^{\beta'} \tag{3}$$

between the absorbed, S_a, and the reemitted, S_r, fluxes; here K_r, α', and β' are certain constants characterizing the wall material. This relationship stems from the family of self-similar solutions for a planar wall, either static[9] or undergoing hydrodynamic expansion,[10] which is heated by an external thermal bath with temperature $T_{\mathrm{ex}}(t)$ varying as a certain power of t.

Evidently, Eq. (3) may become very inaccurate when the time variation of T_{ex} deviates from the power law, with a typical example of T_{ex} remaining more or less constant for a certain period of time (like during the foot of the driving pulse in indirect drive ICF targets[2]) and then rising suddenly to a new value, which persist for some time later. Here it is demonstrated that the accuracy of the view factor method can be improved dramatically if, instead of Eq. (3), one uses the equations

$$S_r(t,\mathbf{r})=K_r[E_a(t,\mathbf{r})]^{\alpha}[S_a(t,\mathbf{r})]^{\beta}, \tag{4}$$

$$\frac{\partial E_a(t,\mathbf{r})}{\partial t}=S_a(t,\mathbf{r}), \tag{5}$$

 1070-664X/96/3(11)/4148/8/$10.00

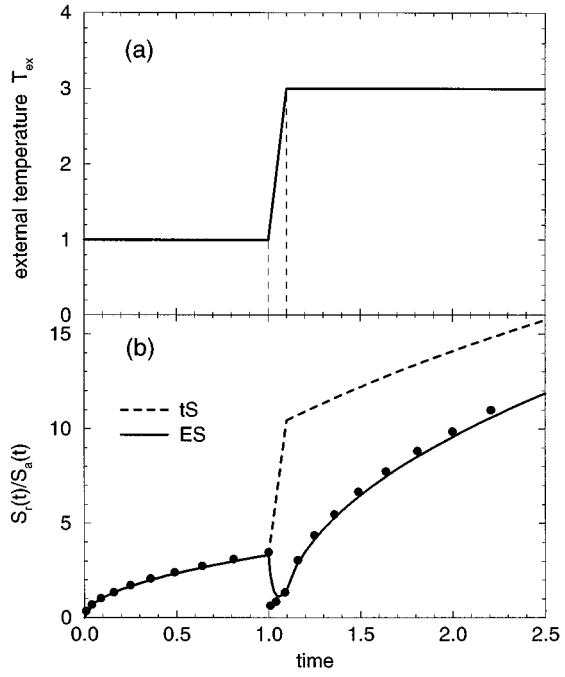

FIG. 1. (a) Time dependence of the boundary temperature $T_{\rm ex}$ for the test problem (6)–(10). (b) Ratio between the reemitted S_r and the absorbed S_a energy fluxes as calculated (i) by numerically solving Eq. (6)—black dots, (ii) in the tS approximation—dashed curve, and (iii) in the ES approximation—solid curve.

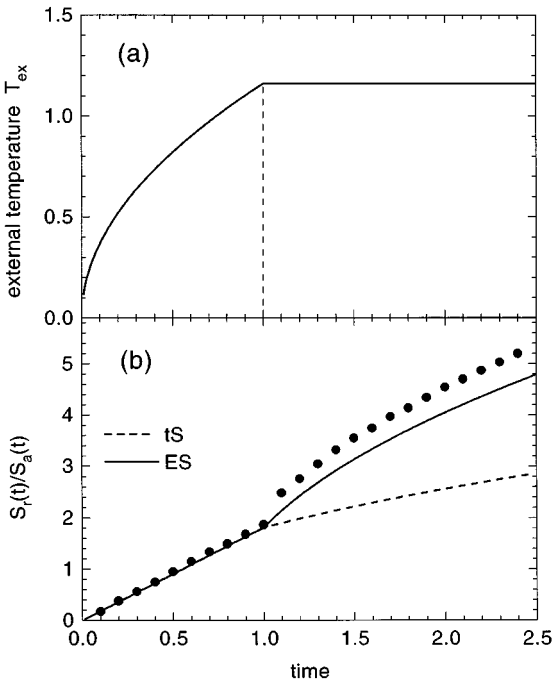

FIG. 2. The same as Fig. 1 but for the boundary temperature $T_{\rm ex}(t)$ varying as shown in part (a) of this figure.

to relate S_r and S_a. Below we refer to Eq. (3) as a ''tS'' approximation, and to Eqs. (4) and (5) as an ''ES'' approximation.

As an illustrative example, consider penetration of a planar heat wave into a motionless wall (hydrodynamic expansion is not relevant for the present argument: when accounted for, it only changes the values of K_r, α, and β) heated by an external source with temperature $T_{\rm ex}(t)$ which varies in time as shown in Fig. 1(a). In many cases of practical interest such a heat wave can be described by the heat conduction equation

$$\epsilon_* \frac{\partial T^\mu}{\partial t} = \frac{\partial}{\partial x}\left(\kappa_* T^n \frac{\partial T}{\partial x}\right), \tag{6}$$

where $\epsilon_* T^\mu$ is the specific (per unit volume) energy of the wall material, and $\kappa_* T^n$ is the heat conduction coefficient. When a boundary condition

$$S_a(t) \equiv -\kappa_* T^n \left.\frac{\partial T}{\partial x}\right|_{x=0} = S_0 t^q \tag{7}$$

is imposed, Eq. (6) admits a self-similar solution which yields the reemitted flux in the form

$$S_r(t) \equiv \sigma T^4(t,0) = \sigma \overline{T_0^4}\left(\frac{t S_a^2(t)}{(q+1)\epsilon_* \kappa_*}\right)^{4/(n+\mu+1)} = \sigma \overline{T_0^4}\left(\frac{E_a(t) S_a(t)}{\epsilon_* \kappa_*}\right)^{4/(n+\mu+1)}, \tag{8}$$

where σ is the Stefan–Boltzmann constant, and $T_0 = T_0(\mu,n,q)$ is a slowly varying dimensionless parameter that should be calculated by solving numerically the eigenvalue problem for the ordinary differential equation to which Eq. (6) is reduced. For the case of $\mu=1$, $n=4$, $q=-1/2$ considered below, $T_0=1.329$. One can use either the ''tS'' form of Eq. (8) to find the values of K_r, α', and β' for the Eq. (3), or its ''ES'' form to determine the values of K_r, α, and β for the Eq. (4).

Figure 1(b) shows the comparison between the tS and ES approximations for a particular case of $\sigma=\kappa_*=\epsilon_*=\mu=1$. The exponent q in Eq. (7) was set equal to $-1/2$, so that the $T_{\rm ex}(t)=$constant phase is reproduced exactly by both the tS and ES approximations. As a result, in the tS approximation we calculate

$$S_r(t)/S_a(t) = \overline{T_0^3}\sqrt{2t}\,T_{\rm ex}(t) \tag{9}$$

[the dashed line in Fig. 1(b)], while the ES equations yield

$$S_r(t)/S_a(t) = \overline{T_0^3} T_{\rm ex}^{-2}(t)\left(2\int_0^t T_{\rm ex}^6(t')\,dt'\right)^{1/2} \tag{10}$$

[the solid line in Fig. 1(b)]. The black dots in Fig. 1(b) represent the numerical solution of the partial differential equation (6) with the boundary temperature as given in Fig. 1(a). One clearly sees that at times $1<t\lesssim 1.5$ the error of the tS approximation is in excess of 100%, while the ES curve is hardly distinguishable from the solution of the diffusion equation (6).

Figure 1 illustrates one characteristic example of a non-power-law time dependence of the source power, when it rises steeply to a new level. Intuitively, it is clear that the ES method will be always superior to the tS approximation in any such situation simply because the absorbed energy E_a is a better measure of the diffusive saturation of the heat wave with respect to the new power level than the time t elapsed from the initial power onset. Figure 2 shows another charac-

TABLE I. Equation-of-state, opacity, and reemission parameters for a selection of elements with different Z.

Parameter	Be	C	Al	Fe	Au
ϵ_* (10^{14} g$^{\nu}$ cm$^{2-3\nu}$ s^{-2} keV$^{-\mu}$)	9.4	11.1	12.5	14.2	11.5
l_* (g^{ν_R} cm$^{1-\nu_R}$ keV$^{-\mu_R}$)	50	70	5.0	0.0027	0.003
μ	1.0042	1.025	1.145	1.327	1.525
ν	0.0024	0.013	0.063	0.120	0.157
μ_R	3.9	5.5	3.8	0.58	1.25
ν_R	1.8	1.8	1.5	1.32	1.2
$\overline{T_0}$	1.032	1.057	1.079	1.078	1.113
K_r	0.47	1.21	1.34	5.08	14.1
α	0.395	0.339	0.399	0.573	0.510
β	0.714	0.620	0.648	0.881	0.748

teristic case, when the initially steep rise of the external temperature, $T_{\rm ex}(t)\propto t^{1/2}$ [$q=1$ in Eq. (7)], is followed by a plato with $T_{\rm ex}(t)=$constant. Again, the advantage of the ES approximation is quite conspicuous. A test case with a sudden drop of the source power would be of no practical interest because both the tS and ES approximations fail to reproduce the behavior of the reemission factor S_r/S_a under such conditions, when the absorbed flux S_a becomes very low and a heated wall radiates back its stored energy.

III. REEMISSION COEFFICIENTS

The values of the reemission parameters K_r, α, and β in Eq. (4) can be determined by either fitting the results of one-dimensional numerical simulations of radiatively driven ablation waves,[4] or by using a suitable self-similar solution. Here we use the Pakula–Sigel[10] self-similar solution, which describes an ablation wave driven into an initially dense planar wall by radiative heat conduction. In contrast to the simple conduction equation (6), this solution accounts for the effect of hydrodynamic expansion on the reemission properties of an ablated surface.

Equations of hydrodynamics with radiative heat conduction admit a self-similar solution when the equation of state and the Rosseland mean free path are approximated as power law functions of temperature and density:

$$\epsilon=\frac{pV}{\gamma-1}=\epsilon_* T^{\mu}V^{\nu}, \tag{11}$$

$$l_R=l_* T^{\mu_R}V^{\nu_R}. \tag{12}$$

Here ϵ is the specific internal energy, p is the pressure, T is the temperature, $V\equiv 1/\rho$ is the specific volume, $\gamma=1+\nu/(\mu-1)$ is the adiabatic index, ϵ_*, l_*, μ, ν, μ_R, and ν_R are the fit parameters. From pure dimensional considerations, one can obtain the following expression for the reemitted radiation flux:

$$S_r=\sigma\overline{T_0^4}\left[\left(\frac{E_a}{\kappa_*}\right)^{1-(3/2)\nu}\frac{S_a^{\nu_R-(1/2)\nu}}{\epsilon_*^{(3/2)\nu_R-(1/2)}}\right]^{4\Lambda}, \tag{13}$$

where

$$\kappa_*=\frac{16}{3}\sigma l_*, \quad \Lambda=\frac{2}{(2-3\nu)(\mu_R+4)+\mu(3\nu_R-1)}, \tag{14}$$

and $\overline{T_0}$ is a dimensionless constant that should be determined by solving numerically the corresponding eigenvalue problem. Below we use the value of T_0 calculated for a constant value of the absorbed flux S_a. This particular case of the Pakula–Sigel solution is appropriate for closed hohlraums heated by ion beams, whereas open hohlraums driven by laser beams might be more adequately described by a solution with a constant boundary temperature, i.e., by somewhat different value of T_0. From Eq. (13) one calculates readily the values of K_r, α, and β that are needed in the Eq. (4). Note that, in their original publication, Pakula and Sigel used the equation of state with $\nu=0$, which is thermodynamically inconsistent for $\mu\neq 1$.

Table I lists the values of the fit parameters in Eqs. (11) and (12) as calculated for the temperature and density intervals 100 eV$\leqslant T\leqslant$300 eV, $0.03\rho_0\leqslant\rho\leqslant 0.3\rho_0$ (ρ_0 is the normal density) for five elements throughout the periodic table, together with the values of T_0, K_r, α, and β. It is assumed that S_r and S_a in Eq. (4) are measured in 10^{14} W/cm^2, and E_a in MJ/cm^2. The values of ϵ_*, α, and β have been calculated by using the mean-ion model from Ref. 11. The Rosseland mean free path l_R was evaluated in the framework of the screened hydrogenic model with l-splitting as described by Rickert and Meyer-ter-Vehn.[12] For aluminum and iron, the power law fit (12) with l_*, μ_R, and ν_R from Table I corresponds to somewhat narrower temperature intervals of 100 eV$\leqslant T\leqslant$200 eV and 100 eV$\leqslant T\leqslant$250 eV, respectively. One sees that the values of T_0, as determined for $S_a=$constant, are very close to unity and change very little from element to element. The latter means that in practice one does not even have to solve the eigenvalue problem and can simply set $T_0=1.0$–1.1.

IV. RADIATIVE SYMMETRIZATION IN CYLINDRICAL HOHLRAUMS

A. Fixed brightness distribution over the hohlraum wall

Within the view factor approach, analysis of radiative symmetrization in a hohlraum can be conducted in two stages.

(i) Given an instantaneous brightness distribution over the inner surface of the hohlraum wall, one can evaluate the uniformity of the incident flux on the surface

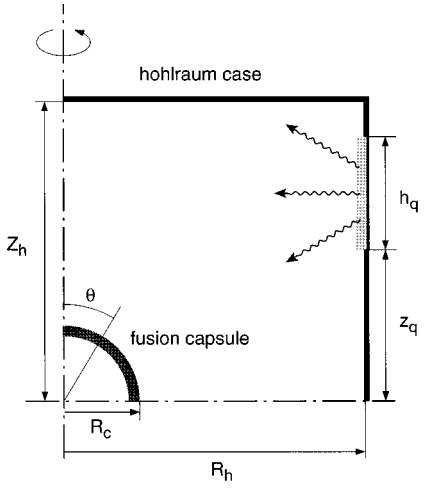

FIG. 3. Schematic one-quarter cut view of a closed cylindrical hohlraum heated by two x-ray ring sources on its sidewall. The configuration is symmetric with respect to the horizontal midplane.

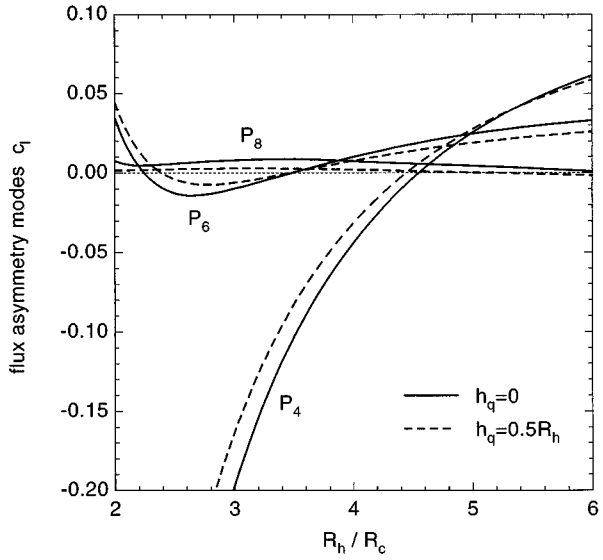

FIG. 4. Legendre components c_l of irradiation nonuniformities along the capsule surface at $t=0$ vs the case-to-capsule radial ratio R_h/R_c in the hohlraum depicted in Fig. 3. The $l=2$ mode is eliminated by a suitable choice of z_q. Good agreement between the dashed and solid curves demonstrates low sensitivity to the width h_q of the source rings.

of spherical fusion capsule for the same moment of time (retardation due to the finite velocity of light is neglected; a single photon pass calculation).

(ii) Given the spatial distribution and temporal evolution of the brightness of the x-ray sources, one calculates the time-dependent asymmetry on the capsule.

In this subsection, we present some results of single pass calculations; the time-dependent aspects are addressed in Sec. IV B. Our analysis is restricted to two-dimensional axisymmetric cylindrical hohlraums.

An axisymmetric distribution of radiation energy flux incident upon a spherical capsule surface can be decomposed in terms of the Legendre polynomials,

$$S_i(\theta)\equiv S_a(\theta)+S_r(\theta)=S_{i0}\left(1+\sum_{l=1}^{\infty} c_l P_l(\cos\theta)\right), \quad (15)$$

and the behavior of individual Legendre modes can then be examined separately. A detailed single pass analysis of radiative symmetrization in closed spherical hohlraums was performed by Murakami and Nishihara[13] and by Caruso and Strangio.[14] In spherical hohlraums, any given Legendre mode l on the hohlraum wall gives rise to the same mode l on the capsule, but with a reduced amplitude; different modes are not coupled to one another. Hence, it is sufficient to calculate the reduction factor for each mode l as a function of the hohlraum-to-capsule radial ratio R_h/R_c. This, however, is not the case for cylindrical hohlraums,[15,2] where, for example, any even mode P_{2k} on the casing wall generates a whole spectrum of even modes on the capsule. Also, spherical harmonics are not a natural basis to decompose functions defined on a cylindrical surface.

Here, instead of individual Legendre components, we consider the following simple mode of the nonuniform brightness distribution over the cylindrical hohlraum case: X rays are emitted uniformly from the surface of two bright circular bands of width h_q on the inner wall of the cylindrical case, as shown in Fig. 3. The rest of the case wall is supposed to be black. A full symmetry across the horizontal midplane is assumed, so that all odd modes in the decomposition (15) vanish. Such a brightness distribution, with an infinitely sharp contrast between the source region and the rest of the hohlraum wall, corresponds to the initial state of both closed and open hohlraums at $t=0$, just after the turn on of the driving power, and gives a good feeling for dominating asymmetry modes in realistic situations.

A general property of hohlraums is that the radiative symmetrization is the least efficient for the lowest spherical harmonics. Hence, the lowest angular modes should be suppressed by adjusting the hohlraum proportions and positions of the x-ray sources. In our case, the distance z_q of the source rings from the midplane can always be chosen such as to eliminate the $l=2$ asymmetry component on the capsule. Depending on the value of h_q/R_h, this occurs at a value of the illumination angle $\theta_q=\arctan\,[R_h/(z_q+\frac{1}{2}h_q)]$ close to 54°–57°. The next even mode $l=4$ is controlled by the ratio R_h/R_c between the case and the capsule radii. Figure 4 shows the amplitudes of the $l=4$, 6, and 8 modes as functions of R_h/R_c for two values of h_q. Along the curves in Fig. 4 the parameter z_q is adjusted such as to zero the $l=2$ mode (the corresponding value of the illumination angle θ_q changes slightly with the value of R_h/R_c).

An important conclusion to be drawn from Fig. 4 is that the $l=4$ mode vanishes in cylindrical hohlraums with $R_h/R_c\approx 4.5$ (compare with $R_h/R_c=4.96$ in spherical hohlraums[13,14]). One readily verifies that this special value of R_h/R_c is rather insensitive to the width of the source rings h_q and their brightness profile. One sees also that at lower values of $R_h/R_c\lesssim 4$—which would be preferred from the point of view of the energy coupling efficiency—the $l=4$ asymmetry mode poses a serious danger for the fusion capsule performance. The higher $l\geqslant 6$ modes are typically below 1%

and not expected to be harmful. There are two possible ways to suppress the $l=4$ mode at $R_h/R_c<4$: (i) to increase the number of source rings, and (ii) to introduce additional elements, such as radiation shields, into the hohlraum. The first method has been employed for the laser driven NIF target,[2] but is presently considered unpractical for the heavy ion fusion because of too much mass required for the x-ray converters. Hence, ion driven cylindrical hohlraums without radiation shields should resort to an option of larger sizes $R_h/R_c \gtrsim 3$–4.

B. Time-dependent asymmetries

As the hohlraum heats up, the nonuniformities of the radiation field on the capsule change in time due to the two main effects: (1) initially dark portions of the hohlraum wall become brighter; (2) a hot plasma blows off the hohlraum and capsule surfaces, which causes the effective hohlraum geometry to change. Here we consider only the first of these two effects and assume that the positions of all the absorbing and reemitting surfaces are fixed in time.

Because of the mode coupling, temporal behavior of asymmetry modes in closed cylindrical hohlraums differs qualitatively from that in closed spherical hohlraums. In particular, if the $l=2$ and 4 modes have been zeroed in a spherical hohlraum with $R_h/R_c=4.96$ at $t=0$ by proper placing of two bright rings, they do not reappear later. This, however, is not the case for cylindrical hohlraums, where temporal variations of the $l=2$ and 4 modes are usually inevitable. Also, there is a considerable difference between the open (with laser entrance hole) and closed cylindrical hohlraums. The physics of open hohlraums has recently been discussed in detail by Lindl.[2] We focus our attention on closed cylindrical hohlraums that may find applications in ion driven targets, whereas certain key characteristics of the open NIF hohlraum are used as a reference case.

The calculations discussed below have been performed with the two-dimensional view factor code VF2 based on Eqs. (1), (2), (4), and (5). This code takes a proper account of the shading effects by all physical surfaces in the hohlraum. In all the cases considered, the capsule radius was fixed at $R_c=1.11$ mm, and the x-ray drive power was chosen in the form

$$W_x(t)=\begin{cases} W_1, & 0<t<t_1, \\ W_1 \exp[(t-t_1)/\Delta t_{12}], & t_1<t<t_2, \\ W_2=W_1 \exp[(t_2-t_1)/\Delta t_{12}], & t_2<t<t_3, \end{cases} \tag{16}$$

which reproduces in an approximate manner the general features of the NIF pulse shape;[2] here $t_1=10$ ns, $t_2=15$ ns, $\Delta t_{12}=1.278$ ns, $t_3=17$ ns, $W_1=6.256$ TW. The total input energy $E_x=\int W_x dt=1.08$ MJ corresponds to the 80% conversion efficiency into x rays of the 1.35 MJ of the driver energy.

As a first example, consider an open hohlraum with the dimensions of the NIF target, namely $R_h=2.75$ mm$\approx 2.5R_c$, $z_h=4.75$ mm, and with the entrance holes of radius $\frac{1}{2}R_h$.[2] Our goal here is not to give a direct comparison with asymmetries calculated for the NIF target (the results published so far on the NIF target would anyhow not be sufficient for such a comparison) but rather to provide a reference case for subsequent discussion of closed hohlraums for heavy ion fusion. Hence, we assume that this hohlraum is heated by two x-ray ring sources of width $h_q=0.5R_h=1.375$ mm, placed symmetrically with respect to the midplane (the actual NIF hohlraum is irradiated by four cones of laser beams, with independent power histories for different pairs of them[2]). The x-ray sources are modeled as two imaginary surfaces on top of the inner case surface, which emit equal amounts of radiation on both their sides in accordance with the Lambertian law. Gold and carbon were used as the case and capsule materials. The reemission properties of these materials were described by the parameters from Table I.

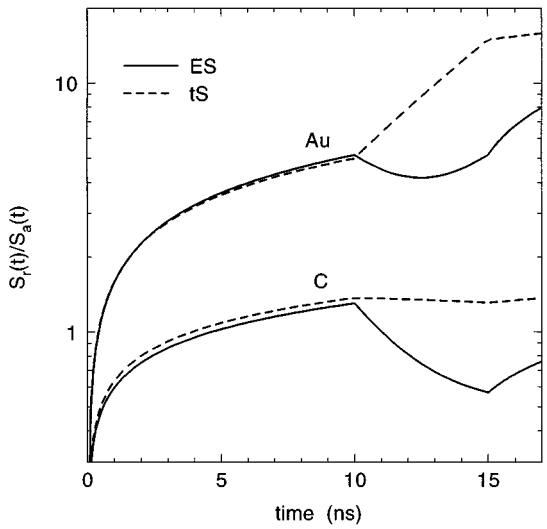

FIG. 5. Temporal evolution of the reemission factor for the gold case and carbon capsule at the midplane of the open NIF hohlraum (Ref. 2) heated by two x-ray rings of width $h_q=0.5R_h=1.375$ mm. The location of the source rings is chosen such as to minimize the $l=2$ asymmetry variations. Note the significant difference between the tS and ES approximations during the steep rise of the pulse power as given by Eq. (16).

Figure 5 shows the temporal behavior of the reemission factor $N_r \equiv S_r/S_a$ [the wall albedo is given by $N_r/(N_r+1)$] for the gold case and carbon capsule as calculated at the midplane cross section of the hohlraum. Note that the dashed curves, calculated with the tS equation (3), deviate by more than a factor of 2 from the solid curves, obtained with the more accurate ES equations (4) and (5), during the transition period from the prepulse to the main pulse. The temporal variation of the P_2 and P_4 asymmetry modes on the capsule is displayed in Fig. 6. Because the hohlraum wall is rather close to the capsule, the amplitude of the P_4 component stays well on the negative side and saturates at a level of $c_4 \approx -10\%$. The latter value (in absolute magnitude) is about a factor of 3 lower than the one calculated for $t=0$ in Sec. IV A (see Fig. 4), a clear manifestation of the radiative smoothing due to the multiple reemission by the hohlraum walls.

Besides the amplitude of irradiation nonuniformities, an important characteristic of a hohlraum is the fraction of the x-ray energy transferred into the capsule. In our simulation of the NIF hohlraum this fraction amounts to $\eta_h=0.18$ (196 kJ out of 1.08 MJ), with the maximum x-ray temperature of

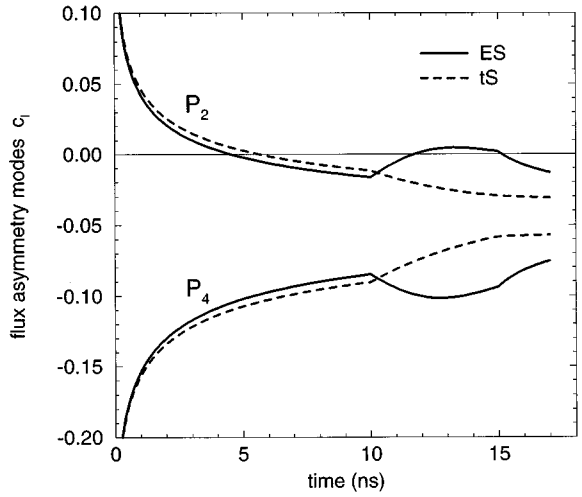

FIG. 6. Time-dependent asymmetry of capsule irradiation in the lowest $l=2$ and 4 Legendre modes as calculated for the open NIF hohlraum heated by two x-ray rings placed symmetrically with respect to the midplane such as to minimize the $l=2$ asymmetry variations.

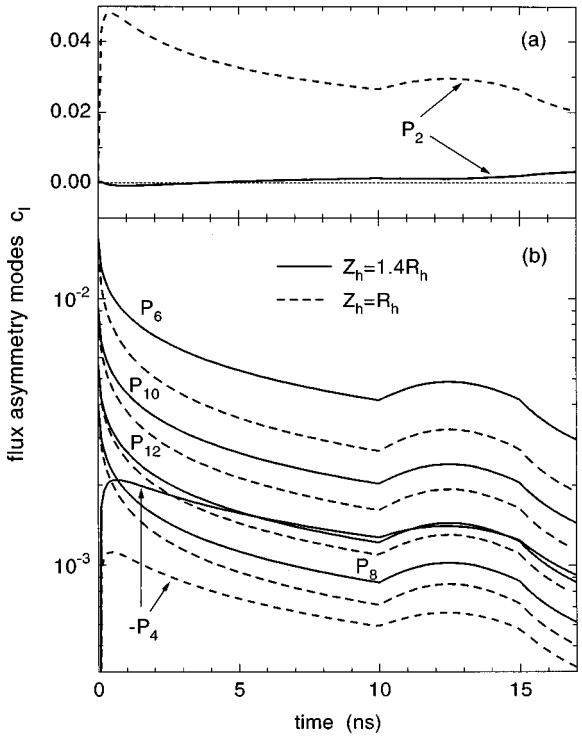

FIG. 7. Temporal variation of Legendre asymmetry modes in a closed cylindrical hohlraum depicted in Fig. 2. The hohlraum radius, $R_h=4.513R_c$, and the location of the source rings, $z_q=0.509R_h$, are fixed such as to start from zero values of the P_2 and P_4 components at $t=0$. The width h_q of the source rings is set equal to $0.3R_h$. It is seen that the P_2 variation is minimized at $Z_h\approx 1.4R_h$, whereas the P_4 variation is not significant and can be ignored.

290 eV. Lindl[2] quotes a lower value of 150 kJ, which may be partly due to a somewhat higher (compared to pure carbon) opacity of the capsule ablator, partly due to a lower than 80% conversion efficiency, and partly due to a decreasing effective surface area of the imploding capsule. Below, when comparing with the NIF target, we assume that its x-ray transfer efficiency is $\eta_h=0.15$–0.18.

In contrast to the laser beams, fast ions do not need entrance holes and can penetrate a closed hohlraum directly through its walls. Hence, closed cylindrical hohlraums deserve special attention as an option for ICF targets driven indirectly by ion beams.

As already discussed before, in a closed cylindrical hohlraum heated by two ring sources of x rays (see Fig. 3) the $l=2$ and 4 asymmetry components can be zeroed by choosing $(z_q+\frac{1}{2}h_q)/R_h\approx 0.65$ and $R_h/R_c\approx 4.5$ (the exact values depend on the ratio h_q/R_h and the brightness distribution over the source rings). However, because of the mode coupling, these components reappear at later times as the wall albedo increases. Figure 7 displays the temporal behavior of the six lowest nonvanishing asymmetry modes as calculated with the VF2 code for a hohlraum with $R_h=4.513R_c$ and $z_q=0.509R_h$. The latter values ensure that both $c_2(t)$ and $c_4(t)$ start from zero at $t=0$ for uniformly bright source rings of width $h_q=0.3R_h$. Two sets of curves correspond to two different values of the hohlraum half-length, $Z_h=R_h$ and $Z_h=1.4R_h$. It is seen that the temporal variations of P_4 are quite small, within the range of 0.1–0.2% (i.e., well below the P_6 level), and can be ignored. The P_2 variations, on the contrary, can reach $\simeq$5% depending on the value of Z_h. These variations are minimized at $Z_h=1.4R_h$. The latter value of Z_h is not sensitive to the width and the brightness profile of the source rings.

Thus, we find that the time-dependent variations of the $l=2$ and 4 modes can be brought down to a level of $\lesssim\pm 0.3\%$ in a closed cylindrical hohlraum with the radius $R_h\approx 4.5R_c$ and the half-length $Z_h\approx 1.4R_h$. Such a hohlraum has at least a factor of 2.7 larger case-to-capsule surface area ratio than the NIF hohlraum. As a result, its energy transfer efficiency, $\eta_h=10\%$, as calculated with the VF2 code for a beryllium capsule with the x-ray pulse profile given by Eq. (16), is at least a factor of 1.5 lower than that for the NIF hohlraum. The x-ray temperature peaks at $T_{x,\max}=240$ eV.

One more conclusion that can be inferred from the plots in Fig. 7 is that, due to multiple reemission by the hohlraum walls, the individual asymmetry components are smoothed down from their initial values by approximately the same factor of 3–4, independent of the mode number. Similar smoothing factors have been obtained earlier by Murakami and Meyer-ter-Vehn[5] and by Temporal and Atzeni[16] for spherical and nearly spherical hohlraums.

The hohlraum configuration with minimized $P_{2,4}$ variations described above may be not quite practical because of a low energy coupling efficiency η_h. In reality, one has to compromise between higher values of η_h and a certain tolerable level of low-mode irradiation asymmetries. A reliable answer can only be obtained in two- or three-dimensional integrated hydrodynamic simulations with radiation transport. Here we present the results of the view factor simulations for a series of closed cylindrical hohlraums with decreasing radial proportion R_h/R_c. As a measure of time-integrated asymmetry, Fig. 8 displays the $l=4$ and 6 modes in the angular decomposition of the total radiation energy E_a absorbed by the capsule for the entire x-ray pulse (16). Given

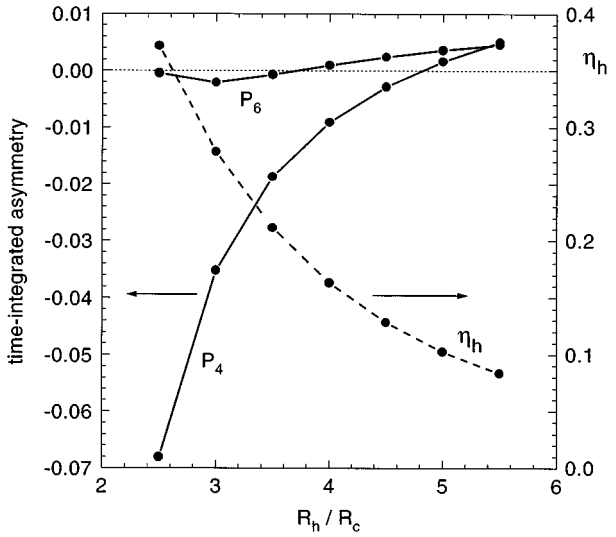

FIG. 8. Legendre components of nonuniformities in the total energy E_a absorbed by the capsule (left ordinates), and the x-ray energy transfer efficiency (right ordinates) vs the case-to-capsule radial ratio R_h/R_c in the closed cylindrical hohlraum. The source rings are placed such as to eliminate the P_2 component in the time-integrated asymmetry.

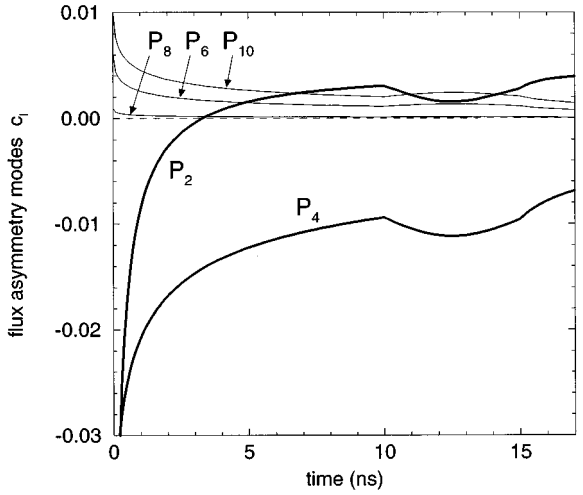

FIG. 9. Time-dependent asymmetry of capsule irradiation in a closed cylindrical hohlraum with $R_h=4R_c$, $Z_h=R_h$. The x-ray transfer efficiency of this hohlraum is $\eta_h=0.16$.

also in Fig. 8 is the fraction η_h of the input x-ray energy absorbed by the capsule. As before, the hohlraum is irradiated by uniformly bright x-ray rings of width $h_q=0.3R_h$, placed such as to zero the P_2 component in the angular decomposition of E_a. The half-length of the hohlraum is fixed at a value of $Z_h=R_h$. Beryllium is taken as the capsule ablator material.

Figure 8 shows how both the energy coupling efficiency η_h and the amplitude of the P_4 asymmetry mode increase with the decreasing R_h/R_c. The best compromise depends on the maximum P_4 amplitude that can be tolerated by the fusion capsule. If the capsule can withstand a 1% time-integrated P_4 perturbation, one can use a cylindrical hohlraum with $R_h/R_c=4$, which has about the same x-ray coupling efficiency, $\eta_h=0.16$, as the much tighter NIF hohlraum. Temporal variations of the P_{4-10} modes in the incident flux for this particular case are shown in Fig. 9. Within the first nanosecond, the P_2 component is reduced to a $\lesssim 1\%$ level, and stays at $|c_2(t)|<0.5\%$ after $t=2$ ns. The P_4 component remains always negative and gradually saturates at a level of $c_4\approx -1\%$.

V. CONCLUSIONS

The system of view factor equations proposed earlier to simulate radiative energy redistribution in cavities[5,6] demonstrates poor accuracy for pulse profiles with sudden increases in drive power, typical for indirect drive ICF targets. This shortcoming can be overcome when the simple power law relationship (3) between the absorbed and reemitted fluxes is replaced by a not much more complicated pair of equations [Eqs. (4) and (5)]. The parameters K_r, α, and β, which characterize the reemissivity of the surface materials and enter Eq. (4), can be evaluated from the Pakula–Sigel self-similar solution without even solving the corresponding eigenvalue problem, provided that the power law interpolations for the equation of state and the Rosseland mean free path are known.

In contrast to the open laser driven hohlraums with holes for the laser beams, ICF targets driven by particle beams can utilize closed hohlraums, which are in principle more efficient in confining radiation and smoothing the irradiation nonuniformities on the fusion capsule. Within the view factor approach, we have explored temporal variations of the lowest asymmetry modes in the simplest case of a closed cylindrical hohlraum without radiation shields, heated by two symmetrical sources of x rays. Possible target configurations for heavy ion inertial fusion with hohlraums of this type have been proposed in Refs. 7 and 8. It is found that the variations of the P_2 and P_4 modes are minimized in a hohlraum with the radius $R_h\approx 4.5R_c$ and half-length $Z_h\approx 1.4R_h$ (R_c is the capsule radius). The x-ray energy transfer efficiency of this hohlraum is $\eta_h\approx 10\%$. This result is not likely to alter significantly after the effects of plasma blowoff are taken into account because the very same relative changes of the effective surface areas of the capsule and the hohlraum case, which lead, say, to a reduction of η_h, improve the symmetry and vice versa. In reality, the above quoted proportions $R_h/R_c\approx 4.5$, $Z_h/R_h\approx 1.4$ for the symmetry-optimized hohlraum should correspond to some time-averaged values. It is less clear and remains to be investigated how strongly the amplitudes of the asymmetry mode variations will be affected by the wall motion under the full treatment of the radiation hydrodynamics.

The last issue concerns possible configuration of a hohlraum target for heavy ion fusion. We have found that, in a closed cylindrical hohlraum without radiative shields heated by two x-ray rings a 1% time-integrated asymmetry in the P_4 mode is compatible with the $\eta_h=0.16$ x-ray energy transfer efficiency into a beryllium capsule of the same size as in the NIF target. Again, this result is not expected to be affected

significantly by the wall motion because the same geometric effects, which reduce η_h, improve the symmetry, and vice versa. The time-averaged case-to-capsule radii ratio in such a hohlraum should be close to $R_h/R_c \approx 4$. Thus, under the assumption that the NIF capsule with a beryllium ablator[2] can be ignited with 180 kJ of the x-ray energy under a persistent 1% perturbation in the P_4 mode, our results may serve as an indication for a possible heavy ion target design at the input energy of $E_{\mathrm{dr}} \approx 2$MJ. Here we assume that the efficiency of the ion energy conversion into x rays is about $\eta_x \approx 0.6$, which is at a lower end of the values calculated by Ho *et al.*[17] with the two-dimensional radiation hydrodynamics code.

ACKNOWLEDGMENTS

I wish to thank J. Meyer-ter-Vehn for a number of stimulating discussions and for providing an opportunity to stay at the Max-Planck-Institut für Quantenoptik.

This work was supported in part by the Bundesministerium für Forschung und Technologie (Bonn), by INTAS under Contract No. INTAS-93-2571, by EURATOM, and within the EC network High Energy Density in Matter (Contract No. ERB...CT 930327).

[1] J. Nuckolls, Phys. Today **35**, 24 (1982).
[2] J. Lindl, Phys. Plasmas **2**, 3933 (1995).
[3] R. Sigel, R. Pakula, S. Sakabe, and G. D. Tsakiris, Phys. Rev. A **38**, 5779 (1988).
[4] M. Murakami and J. Meyer-ter-Vehn, Nucl. Fusion **31**, 1315 (1991).
[5] M. Murakami and J. Meyer-ter-Vehn, Nucl. Fusion **31**, 1333 (1991).
[6] G. D. Tsakiris, Phys. Fluids B **4**, 992 (1992).
[7] V. V. Vatulin, V. G. Zagrafov, G. N. Remizov, G. I. Skidan, and S. I. Skrypnik, ''Numerical investigations of performance some design of heavy-ion thermonuclear fusion target,'' presented at the International Symposium on Heavy Ion Inertial Fusion, Princeton, 6–9 September 1995, submitted to Fusion Eng. Design.
[8] M. M. Basko, M. D. Churazov, and D. G. Koshkarev, ''ITEP conception of a heavy ion fusion facility,'' to appear in Fusion Eng. Design (1996).
[9] Ya. B. Zel'dovich and Yu. P. Raiser, *Physics of Shock Waves and High-Temperature Hydrodynamic Phenomena* (Academic, New York, 1966), Sec. II.10.
[10] R. Pakula and R. Sigel, Phys. Fluids **28**, 232 (1985).
[11] M. Basko, Teplofiz, Vys. Temp. **23**, 483 (1985) [High Temp. (USSR) **23**, 388 (1985)].
[12] A. Rickert and J. Meyer-ter-Vehn, Laser Part. Beams **8**, 715 (1990).
[13] M. Murakami and K. Nishihara, Jpn. J. Appl. Phys. **25**, 242 (1986).
[14] A. Caruso and C. Strangio, Nucl. Fusion **31**, 1399 (1991).
[15] D. W. Phillion and S. M. Pollain, Phys. Plasmas **1**, 2963 (1994).
[16] M. Temporal and S. Atzeni, Nucl. Fusion **32**, 557 (1992).
[17] D. D.-M. Ho, J. D. Lindl, and M. Tabak, Nucl. Fusion **34**, 1081 (1994).